

## Fusion-fission and quasi-fission contribution in decay of heavy mass nuclei

Gurvinder Kaur, Neha Grover, and Manoj K. Sharma\*  
 School of Physics and Materials Science,  
 Thapar University, Patiala - 147004, Punjab, INDIA

### Introduction

The reactions involving heavy mass nuclei are of tremendous importance in understanding the compound nucleus (CN) and non-compound processes (NCN). The evaporation residue and fusion-fission originate from the CN channel whereas quasi fission (QF) and deep inelastic collision (DIC) fall under NCN category. The dynamical non-equilibrium QF process, retains the history of its formation and is largely influenced by entrance channel reaction conditions like charge product ( $Z_1Z_2$ ), mass asymmetry ( $\eta$ ), fissility parameter ( $X_{eff}$ ) etc. It has been observed that the suppression of fusion-fission and onset of quasi-fission is effectively governed by these features. However, exceptions to these conditions have also been observed [1]. Thus in order to have comprehensive picture of heavy mass nuclei, a thorough description of decay properties associated with them is highly desirable. With this aim, an attempt has been made to observe the relative contribution of fusion-fission and quasi-fission processes in  $^{18}\text{O}+^{197}\text{Au}$  and  $^{36}\text{S}+^{197}\text{Au}$  reactions using dynamical cluster-decay model (DCM) [2, 3].

In the present work, we choose to apply DCM on  $^{215}\text{Fr}^*$  and  $^{233}\text{Am}^*$  nuclei formed at excitation energy,  $E_{CN}^*=60$  MeV. Here our main aim is to account for (i) Relative behavior of  $^{18}\text{O}+^{197}\text{Au}$  channel in reference to earlier investigated reactions  $^{11}\text{B}+^{204}\text{Pb}$  and  $^{19}\text{F}+^{196}\text{Pt}$  [2], forming same compound nucleus  $^{215}\text{Fr}^*$ . (ii) Role of different projectiles on same target under similar reaction conditions (iii) Analysis of fission and QF compo-

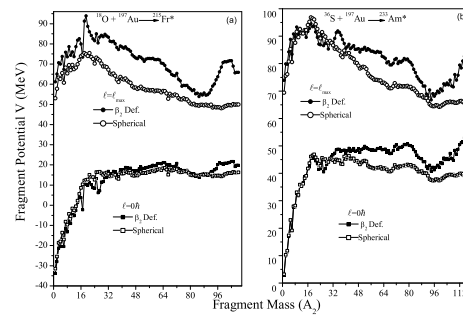


FIG. 1: Fragmentation potential plotted as a function of light fragment mass  $A_2$ , for (a)  $^{215}\text{Fr}^*$  and (b)  $^{233}\text{Am}^*$  nuclei at  $E_{CN}^*=60$  MeV.

nent wherever applicable. It is relevant to mention here that deformation and temperature effects are duly incorporated and decay patterns are investigated using collective clusterization method within the framework of DCM approach

### Dynamical Cluster-decay Model

The DCM based on quantum mechanical fragmentation theory (QMFT) is worked out in terms of collective co-ordinates of mass asymmetry,  $\eta_A = (A_1 - A_2)/(A_1 + A_2)$  (1 and 2 stand, respectively, for heavy and light fragments) and relative separation R. DCM is a two step model where the preformation probability ( $P_0$ ) refers to  $\eta$ -motion and penetrability ( $P$ ) refers to the R-motion. The  $P_0$  is obtained by solving the stationary Schrödinger equation given as,

$$P_0 = |\psi(\eta(A_i))|^2 \sqrt{B_{\eta\eta}} \frac{2}{A_{CN}} \quad (1)$$

While the penetrability  $P$  is calculated using the WKB integral as

$$P = \exp \left[ -\frac{2}{\hbar} \int_{R_a}^{R_b} \{2\mu[V(R) - Q_{eff}]\}^{1/2} dR \right] \quad (2)$$

\*msharma@thapar.edu

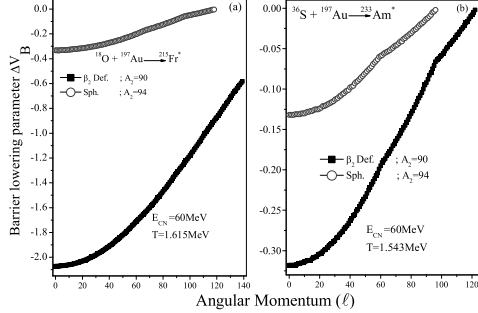


FIG. 2: (a) Variation of barrier lowering parameter plotted as a function of angular momentum for (b)  $^{215}\text{Fr}^*$  and (c)  $^{233}\text{Am}^*$  nuclei.

where  $R_a$  is the first turning point of the barrier penetration. The multipole deformations  $\beta_{\lambda i}$  ( $\lambda=2, 3, 4$ ), and orientations  $\theta_i$  ( $i=1,2$ ) of two nuclei or fragments are incorporated in DCM along with temperature (T) effect. In terms of  $P_0$  and P, using  $\ell$  partial waves, the CN decay cross-section is defined as

$$\sigma = \frac{\pi}{k^2} \sum_{l=0}^{l_{max}} (2l+1) P_0 P; \quad k = \sqrt{\frac{2\mu E_{c.m.}}{\hbar^2}} \quad (3)$$

Here,  $\ell_{max}$  is the maximum angular momentum up to which the cross-section are fitted, and is defined at a point where  $\sigma_{ER} \rightarrow 0$ .

## Results and Discussions

The fragmentation potential V (MeV) plotted as a function of fragment mass  $A_2$ , for  $^{18}\text{O} + ^{197}\text{Au} \rightarrow ^{215}\text{Fr}^* \rightarrow A_1 + A_2$  and  $^{36}\text{S} + ^{197}\text{Au} \rightarrow ^{233}\text{Am}^* \rightarrow A_1 + A_2$  reactions is shown in Fig.1(a) and (b) respectively. To explore role of deformations, the calculations have been carried out for spherical and  $\beta_2$  deformed fragmentation approach. From the figure it is evident that, at  $\ell=0\hbar$  the deformation effects are visible only for heavier nucleus whereas, at higher  $\ell$ -values the same are prominent for both  $^{215}\text{Fr}^*$  and  $^{233}\text{Am}^*$  systems. Also, the mass distribution for both the nuclei changes from symmetric to asymmetric with inclusion of deformations. For spherical choice, the fragments contributing towards the fission decay are  $A_2=85-104$  and  $A_2=92-105$  while for deformed approach they vary from 80-93 and 89-103 for  $^{215}\text{Fr}^*$  and  $^{233}\text{Am}^*$  respectively. The contribution of complementary fragments is duly included in all above consideration.

The DCM has an inbuilt barrier lowering property that is included via the neck-length parameter  $\Delta R$ . Fig.2(a),(b) shows variation of barrier-lowering parameter  $\Delta V_B$ , which is the difference between the actually used barrier  $V(R_a)$  and the top of the calculated barrier  $V_B$ , [ $\Delta V_B = V(R_a) - V_B(\ell)$ ]. For both the nuclei, the magnitude of  $\Delta V_B$  is minimum at higher  $\ell$ -values and increases with decrease in  $\ell$ . Also, the barrier lowering is small in magnitude for spherical choice independent of mass of parent nucleus. However, the difference in  $\Delta V_B$  for deformed and spherical choice is more in  $^{215}\text{Fr}^*$  nucleus and relatively lesser for heavier nucleus  $^{233}\text{Am}^*$ .

For  $^{215}\text{Fr}^*$  nucleus, by taking spherical fragmentation, at neck-length parameter  $\Delta R=1.432\text{fm}$ , the fission cross-section is observed to be 668mb, while with inclusion of deformations, a nice agreement with experimentally measured capture-fission cross-section (834mb) is obtained at relatively smaller  $\Delta R \sim 1.210\text{fm}$ . This suggest that deformations play a significant role in decay of  $^{215}\text{Fr}^*$  nucleus for which no signature of QF is observed as CN channel seem to address the available data. On the other hand, for  $^{233}\text{Am}^*$  nucleus having high charge product ( $Z_1 Z_2$ ) and fissility of the incoming channel [1], the fission contribution is small being 312mb ( $\Delta R=1.426$ ) and 384mb ( $\Delta R=1.408$ ) for spherical and deformed approach respectively, as compared to experimental cross-section (748mb). Consequently, the presence of QF ( $\sigma_{capture-fission}^{expt} - \sigma_{fission}^{DCM}$ ) is estimated for both spherical ( $\sigma_{QF}=436\text{mb}$ ) and deformed ( $\sigma_{QF}=364\text{mb}$ ) approach considered for heavy mass  $^{233}\text{Am}^*$  system. Thus DCM calculations support the presence of QF for relatively heavier nucleus having large entrance channel fissility and the same is absent in case of  $^{215}\text{Fr}^*$ .

## References

- [1] R. Yanez, W. Loveland, J. S. Baret *et al.*, Phys. Rev. C **88**, 014606 (2013).
- [2] Gudveen Sawhney, Gurbinder Kaur, Manoj K Sharma and Raj K Gupta, Phys. Rev. C **88**, 034603 (2013).
- [3] R. K. Gupta, *et al.*, J. Phys.G; Nucl.Part. Phys. **31**, 631 (2005).